

# Solar prominences with Na and Mg emissions and centrally reversed Balmer lines

G. Stellmacher<sup>1</sup> and E. Wiehr<sup>2</sup>

<sup>1</sup> Institute d'Astrophysique (IAP), 98 bis Blvd. d'Arago, 75014 Paris, France

<sup>2</sup> Institut für Astrophysik der Universität, Friedrich-Hund-Platz 1, 37077 Göttingen, Germany

Received June 29, 2004; accepted Oct. 14, 2004

## ABSTRACT

**Aims.** We study spectral lines in exceptionally bright solar limb prominences with pronounced sodium and magnesium emission and central reversion of the first two hydrogen Balmer lines.

**Methods.** We simultaneously measure the line profiles of H $\alpha$ , H $\beta$ , HeD<sub>3</sub>, He II 4685, He I 5015 (singlet), NaD<sub>2</sub> and Mg b<sub>2</sub> using the THEMIS telescope on Tenerife.

**Results.** We find that most prominences with significant NaD<sub>2</sub> and Mg b<sub>2</sub> emission show centrally reversed profiles of H $\alpha$  and occasionally even of H $\beta$ . The strongest emissions reach integrated intensities  $E\beta > 16 \cdot 10^4$  erg/(s cm<sup>2</sup> ster). The centrally reversed profiles are well reproduced by semi-infinite models. The source function reaches  $S_\alpha \leq 36 \cdot 10^4$  erg/(s cm<sup>2</sup> ster Å) corresponding to an excitation temperature of  $T_{ex} \approx 3950$  K; here, the optical thickness of H $\alpha$  amounts to  $\tau \approx 10.0$ . The narrow widths of the NaD<sub>2</sub> and Mg b<sub>2</sub> profiles yield a non-thermal broadening of  $V_{tu} = 5$  km/s.

**Key words.** Prominences - line profiles - line radiance - central reversal - excitation temperature - optical thickness

## 1. Introduction

The simultaneous occurrence of resonance lines with low ionization potential, like Mg b<sub>2</sub> and NaD<sub>2</sub>, and of hydrogen and helium lines with much higher excitation and ionization energy illustrates the large deviation from LTE in atmospheres of solar prominences. Only few comprehensive sets of simultaneous emission data have so far been published, e.g., Yakovkin & Zel'dina (1964), Kim (1987). High precision photometry of prominence spectra show for faint emissions ( $E\beta < 1 \cdot 10^4$  erg/(s cm<sup>2</sup> ster); corresponding to  $\tau_\alpha < 1.0$ ) an empirical relation between H $\alpha$  and H $\beta$  which is independent of the individual prominence (Stellmacher & Wiehr 1994b). For brighter emissions, however, this relation depends on the prominence atmosphere. The present data are considered as an extension toward strongest emissions with  $E\beta > 4 \cdot 10^4$  erg/(s cm<sup>2</sup> ster). Such bright prominences are known to be cool, dense, and rather unstructured (Stellmacher & Wiehr 1995). They allow a determination of upper limits of the H $\alpha$  source function as well as a quantitative analysis of the centrally reversed H $\alpha$  profiles and their representation by models.

## 2. Observations and data reduction

We observed with the French-Italian solar telescope THEMIS simultaneously the emission lines H $\alpha$ , H $\beta$ , HeD<sub>3</sub>, He II 4685, He I 5015 Å (singlet) NaD<sub>2</sub> and Mg b<sub>2</sub> on October 18 and 23, 2000. For the two data sets the entrance slit of 0.5 arcsec and 0.75 arcsec width, respectively, was aligned along the direction of atmospheric refraction (i.e. perpendicular to the horizon). Exposure times of a few seconds

Send offprint requests to: E. Wiehr

Correspondence to: ewiehr@astrophysik.uni-goettingen.de

gave about 2000 counts for the brightest H $\alpha$  and 300 counts for the faintest Mg b<sub>2</sub> emissions.

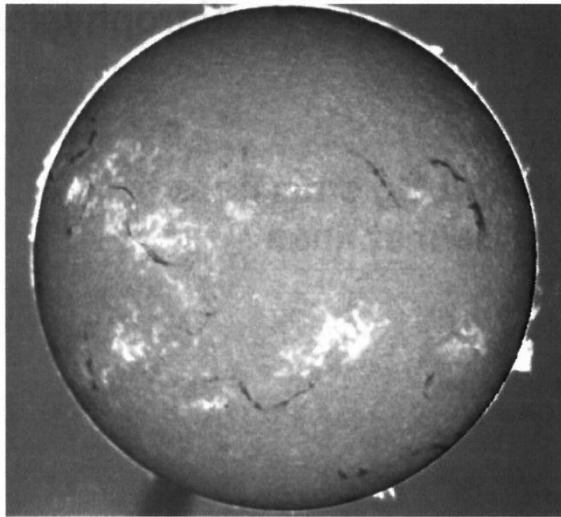
The CCD-images were corrected for the dark and the gain matrices; the underlying stray-light aureole was subtracted using spectra from locations adjacent to the corresponding prominence. For the calibration of the prominence emissions, we took disk-center spectra and use the absolute intensities given by Labs & Neckel (1970) in units of [ $10^6$  erg/(s cm<sup>2</sup> ster Å)]: I(6563 Å) = 2.86, I(5890 Å) = 3.34, I(5876 Å) = 3.36, I(5173 Å) = 3.93, I(5015 Å) = 4.06, I(4861 Å) = 4.16 and I(4685 Å) = 4.3.

We determine the total emission  $E$  ('line radiance') as the intensity integrated over the whole profile of the line:  $E = \int I d\lambda$  [erg/(s cm<sup>2</sup> ster)] and give  $I$  and  $E$  in units of  $10^4$  to enable an easy comparison with former data. H $\alpha$  solar survey images of the prominences under study (Fig. 1) show that these low-latitude objects ( $\vartheta < 32$ ) occurred under various aspect angles between 'face-on' and 'end-on'. An example of simultaneously observed CCD spectra is displayed in Fig. 2.

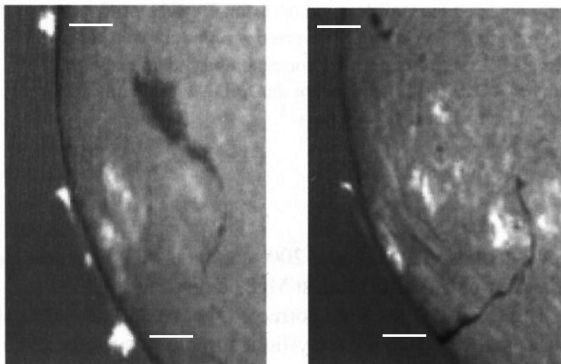
## 3. Results for the H $\alpha$ and H $\beta$ lines

### 3.1. Emission relations

The observed emissions, given in Fig. 3, reach line a radiance up to  $E\beta = 16 \cdot 10^4$  erg/(s cm<sup>2</sup> ster), being four times larger than the maximum values by Stellmacher & Wiehr (1994b; their Figs. 2 and 3). Comparably high values were published by Yakovkin & Zel'dina (1963; entered in Fig. 3). For faint  $E\beta \leq 1 \cdot 10^4$  erg/(s cm<sup>2</sup> ster), our data perfectly match the general empirical relation by Stellmacher & Wiehr (1994b) between  $E_\alpha$  and  $E\beta$  (crosses in Fig. 3). For stronger emissions  $E\beta > 3 \cdot 10^4$  our recent data are slightly



October 18, 2000



October 23, 2000, SE

October 25, 2000, SE

**Fig. 1.**  $H\alpha$  solar survey images (Meudon observatory) with the prominences at E/22°N and W/24°S observed on Oct. 18 (*upper panel*) and on Oct. 23 at the east limb 5°N, 15°S, 23°S and 32°S (*lower left panel*) together with the corresponding disk appearance on Oct. 25 (*lower right panel*).

below that curve. The first Balmer decrement  $E\alpha/E\beta$  shows for the brightest emissions values near 3.0, and limiting values clearly above 10.0 for the faintest emissions. This agrees with Stellmacher & Wiehr (1994b) and follows the curves (also entered in Fig. 3) calculated by Gouttebroze et al. (1993; hereafter referred to as GHV) for temperatures of  $T_{kin} = 4300$  K and, respectively,  $T_{kin} = 6000$  K.

The here obtained values of line radiance well agree with former data from much fainter and more structured prominences, obtained with quite different methods. This indicates that possible influences from 'filling' play a minor role (in agreement with Stellmacher, Wiehr, Dammasch 2003), as is also seen from the independence on the aspect angle: e.g., we do not find significant differences between the 'face-on' prominence at 5°N and the 'end-on' one at 32°S, both at the east limb on Oct. 23 (marked in Fig. 1).

### 3.2. Centrally reversed $H\alpha$ profiles

We observe distinct central reversions (double peaks) of the  $H\alpha$  profile for a line radiance  $E\beta > 5 \cdot 10^4$  erg/(s cm<sup>2</sup> ster).

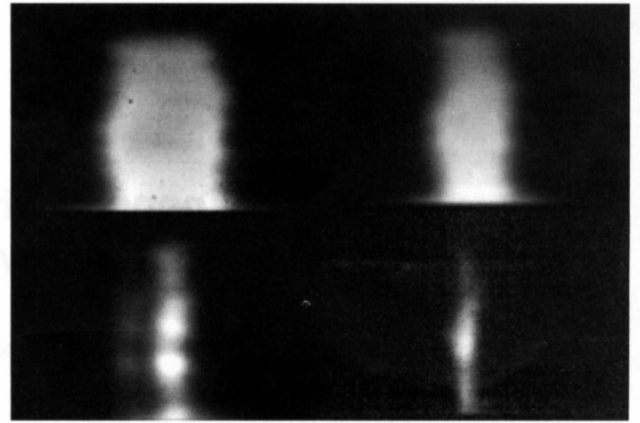


**Fig. 2.** CCD spectra of the Balmer lines  $H\alpha$  (*upper left*),  $H\beta$  (*upper right*), both with central reversions, and the simultaneously observed  $HeD_3$  (*lower left*) and  $NaD_2$  (*lower right panel*), in the prominence at W/24°S on Oct. 18; each sub-image spans 41'' x 2.5Å.

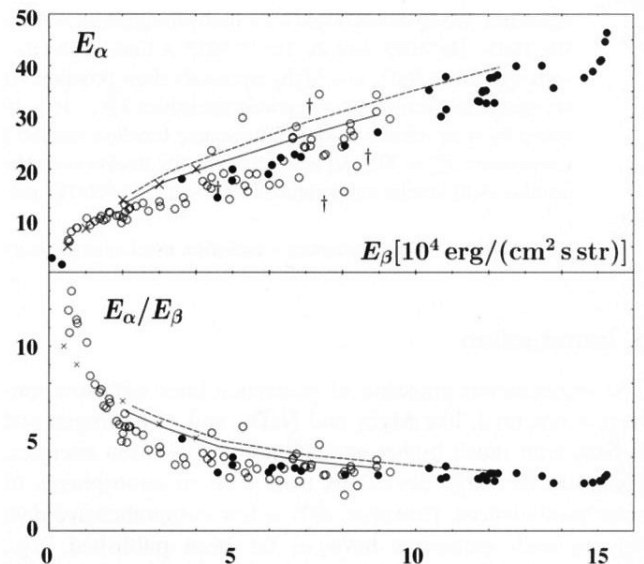


**Fig. 3.** Observed line radiance  $E\alpha$  (*upper*) and 1. Balmer decrement  $E\alpha/E\beta$  (*lower panel*) both versus  $E\beta$ ; prominences with strong central  $H\alpha$  reversion (*filled circles*); mean observations by Stellmacher & Wiehr (1994b) (*crosses*); data by Yakovkin & Zel'dina (1963) (*dags*); model calculations by GHV (1993) for  $T_{kin} = 4300$  K (*solid*) and  $T_{kin} = 6000$  K (*dashed line*).

An example is shown in Fig. 4 together with simultaneously observed He and metal lines. We find the most prominent central reversions in the strongest, yet *narrow* emission profiles. In Fig. 5 we give some relations of the observed reversion signatures and compare them to such from the comprehensive set of  $H\alpha$  emission profiles calculated by GHV for thick slabs of models with  $T_{kin} = 6000 - 8000$  K and  $v_{nth} = 5$  km/s, acting as semi-infinite layers.

Profiles with the most prominent central reversions are markedly narrow, and their signatures (filled circles in Fig. 5) well follow the calculated relations and can thus be explained by pure line-saturation. Data that deviate

from the calculated curves (open circles) are derived from broader line profiles. This stronger broadening (e.g., due to macro velocities or superpositions) will readily lead to a deterioration of the pure saturation effect.

The fact that the bright and rather unstructured prominences show strikingly narrow lines was already mentioned by Stellmacher & Wiehr (1994b). We consider the central reversions as a signature of emission in semi-infinite dense layers. No evident relation is found between the intensity difference of the two emission peaks near line-center. Here, non-LTE transfer calculations should be considered, including 'spatially correlated velocity fields' as suggested by Magnan (1976).

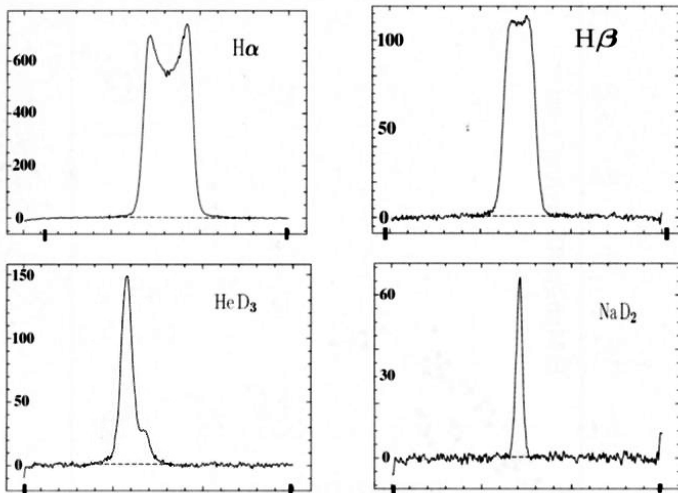


**Fig. 4.** Profiles of simultaneously observed emissions with distinct saturation of H $\alpha$  and H $\beta$  (*upper panels*) together with HeD $_3$  and NaD $_2$  (*lower levels*): ordinates = CCD counts; thick abscissa tick marks give  $\Delta\lambda = 5.0\text{\AA}$ ; (He-CCD misc-entered).

### 3.3. Central intensities and source function

The double peaked H $\alpha$  emission originates from thick layers with  $\tau_0^\alpha \gg 1.0$ , for which the central line intensity becomes  $I_0^\alpha = S^\alpha(1 - e^{-\tau_0^\alpha}) \approx S^\alpha$  allowing us to directly deduce the source function. For the strongest emissions, we find, (following the method described by Stellmacher & Wiehr 1994b; Sect. 4)  $\tau_0^\alpha \gg 5.0$ . If we express the relative level population of the H $\alpha$  transition by the Boltzmann formula:

$$(n_{0,3}g_{0,3})/(n_{0,2}g_{0,2}) = \exp[-hc/(\lambda_\alpha k T_{ex}^\alpha)]$$

and insert this into the general equation for the source function, we obtain the corresponding Planck function,  $B$ , for the excitation temperature  $T_{ex}^\alpha$ :

$$S_\alpha = (2hc^2/\lambda_\alpha^5)/(\exp[-hc/(\lambda_\alpha k T_{ex}^\alpha)] - 1) = B(T_{ex}^\alpha)$$

The mean upper values (open circles in Fig. 6) for non-reversed profiles with  $I_0^\alpha \approx 36 \cdot 10^4 \text{ erg}/(\text{s cm}^2 \text{ ster } \text{\AA})$  correspond to an excitation temperature  $T_{ex}^\alpha \approx 3950 \text{ K}$ . Fainter prominences analyzed by Stellmacher & Wiehr (1994b)

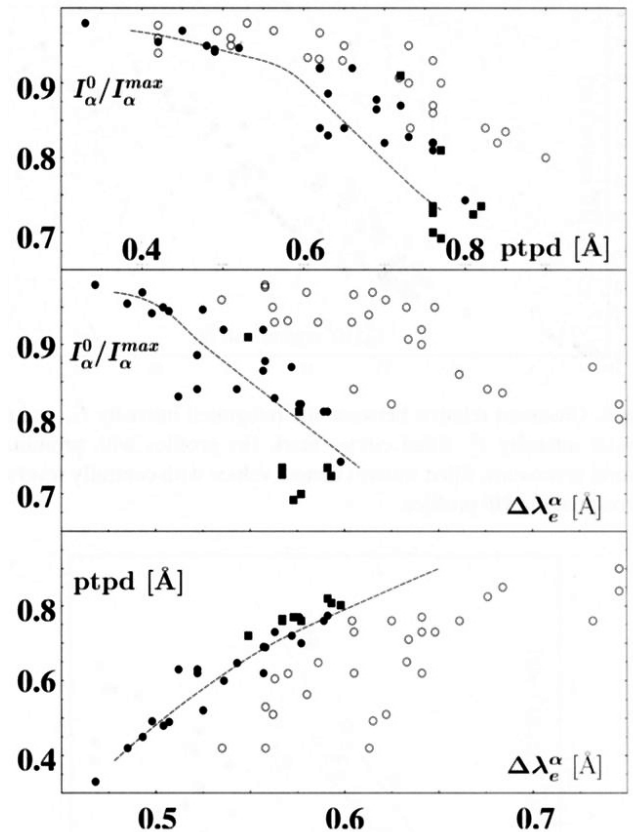


**Fig. 5.** Observed relations of central intensity  $I_0^\alpha$ , peak-intensity  $I_\alpha^{max}$ , peak-to-peak distance ptpd of the two H $\alpha$  maxima, and the half line width  $\Delta\lambda_e$  at  $I_0^\alpha/e$ ; emissions with prominent central reversals are marked by filled circles (as in Fig. 3); filled squares denote values for which corresponding H $\beta$  profile is also centrally reversed. *Dashed lines* give calculations from slab-models by GHV.

gave smaller mean upper values  $I_0^\alpha \approx 26 \cdot 10^4$  corresponding to  $T_{ex}^\alpha \approx 3700 \text{ K}$ . GHV obtain for their models with  $T_{kin} = 6000 \text{ K}$  and  $v_{nth} = 5 \text{ km/s}$  a source function  $S^\alpha = 36 \cdot 10^4$  at  $\tau_0^\alpha = 10$  in good agreement with the present observations (Fig. 6).

The central intensity of the reversed profiles reaches values  $I_{max}^\alpha \approx 43 \cdot 10^4 \text{ erg}/(\text{s cm}^2 \text{ ster } \text{\AA})$  (cf., Fig. 5) which corresponds to  $T_{ex}^\alpha \approx 4000 \text{ K}$ . The two peaks outside the line center arise from smaller  $\tau^\alpha$  values, their higher intensity then indicating an increase of the source function towards the prominence interior (see also Yakovkin & Zel'dina 1964). The model calculations of GHV (1994; their Fig. 18) indicate a rise of  $S^\alpha$  even beyond  $0.16 \cdot I^{phot}$ , i.e.  $S_\alpha > 46 \cdot 10^4 \text{ erg}/(\text{s cm}^2 \text{ ster } \text{\AA})$ ; this conflicts with the occurrence of dark filaments on the disk. Such high  $S^\alpha$  might only be valid for spicules and eruptive objects.

## 4. The helium emissions

The simultaneously observed HeD $_3$  and H $\beta$  lines show distinct branches in their intensity relation (Fig. 7): Emissions from prominence locations with prominent H $\alpha$  reversions show ratios  $E_{HeD3}/E_\beta = 0.2 - 0.3$ , while less thick prominences follow branches with ratios 0.4 - 0.5. This confirms earlier results by Stellmacher & Wiehr (1994a, 1995) who

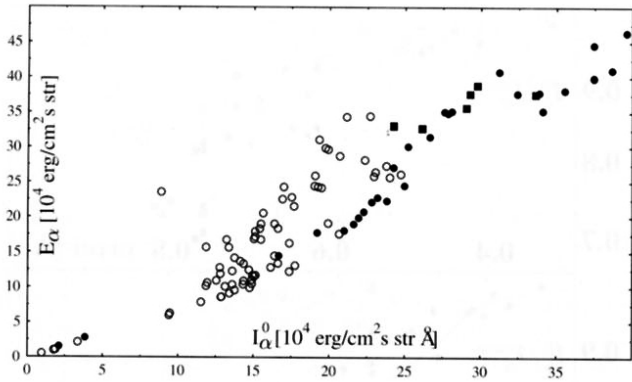


**Fig. 6.** Observed relation between the integrated intensity  $E\alpha$  and the central intensity  $I_\alpha^0$ ; filled circles mark  $H\alpha$  profiles with prominent central reversions, filled squares denote values for which the corresponding  $H\beta$  profile is also centrally reversed.

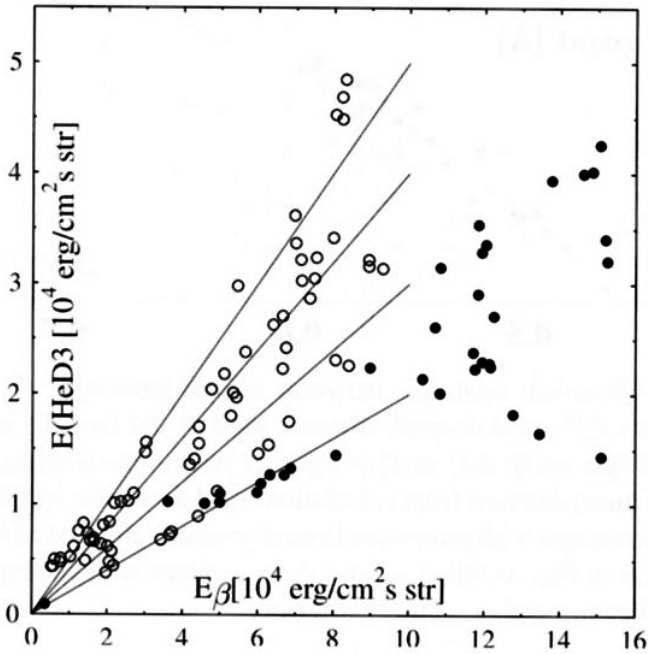


**Fig. 7.** Integrated intensities of  $HeD_3$  and  $H\beta$ ; emissions corresponding to prominent  $H\alpha$  reversions are marked by filled circles; full lines trace emission ratios of 0.5, 0.4, 0.3, and 0.2

found from analyses of  $He\ 3889$  with  $H\ 3888$ , and of  $HeD_3$  with  $H\beta$  that the emission ratio of the He-triplet and the Balmer lines shows typical mean values, in the sense that prominences with stronger Balmer emissions (known to be cooler, less structured, and denser; cf., introduction) yield lowest Helium-to-Balmer ratios.

The  $HeD_3$  fine-structure components can be used to measure of the optical thickness, as was shown by Stellmacher, Wiehr, Dammasch (2003) for the analogous case of  $He\ 10830\text{\AA}$ . In contrast to that triplet line,  $HeD_3$  does not allow us to determine the ratio of the faint red component and the two (not separated) main components with similar reliability, due to the much smaller spectral

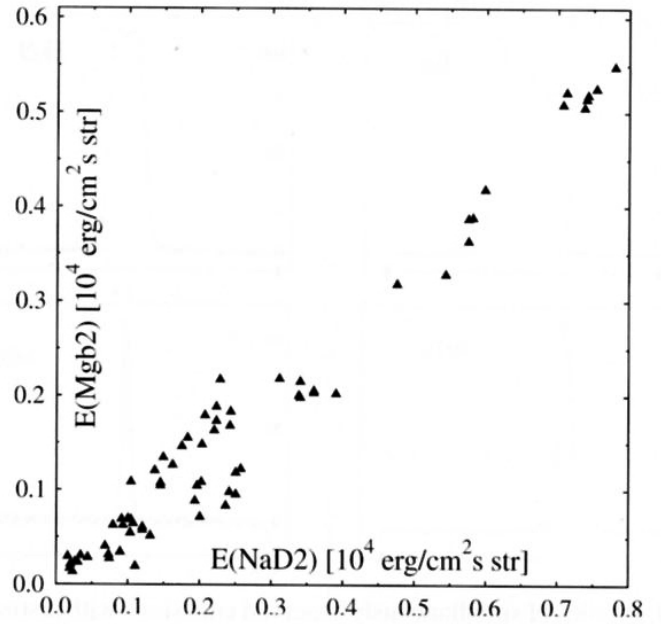


**Fig. 8.** Emission relation of  $Mgb_2$  and  $NaD_2$ .

distance of only  $0.32\text{\AA}$ . The ratio 1 : 8 for the optically thin case increases up to 1 : 6 for emissions  $E_{HeD_3} \geq 0.6 \cdot 10^4$  erg/(s cm<sup>2</sup> ster), indicating that  $HeD_3$  begins to saturate.

Our instrumental set-up also covers the lines  $He\ II\ 4685.7$  and  $He\ I\ 5015.7$  (singlet). We do not find any significant  $He\ II$  emission in the prominences observed, which may be too cool and dense for sufficient  $He\ II$  excitation. The faint  $He\ I$  singlet line was only measurable in one prominence, its width is quite similar to that of  $HeD_3$ , yielding  $(\Delta\lambda/\lambda_0)^{He\ I} \leq 2.7 \cdot 10^{-5}$ . The integrated intensity  $E(He\ 5016) \approx 0.05 \cdot 10^4$  erg/s cm<sup>2</sup> ster gives an emission ratio with  $HeD_3$  of  $He^{singl}/He^{tripl} \approx 0.016$ . Other line combinations, including the stronger singlet line  $He\ 6678$ , might be useful to extend the study of singlet-to-triplet ratio by Stellmacher & Wiehr (1997).

### 5. Emissions of the metal lines $Mgb_2$ and $NaD_2$

The integrated intensities of  $Mgb_2$  and  $NaD_2$  show a linear relation with a ratio  $E(Mgb_2)/E(NaD_2) = 0.7$  (Fig. 8), indicating that the emissions of both lines are closely related. Their integrated intensities strongly depend on the prominence thickness, as can be seen from the relation with  $H\beta$  in Fig. 9. We observe reliable emissions of  $NaD_2$  only if  $E_\beta > 3 \cdot 10^4$  erg/s cm<sup>2</sup> ster. Maximum  $E(NaD_2) \approx 0.78 \cdot 10^4$  erg/s cm<sup>2</sup> ster is observed at prominence locations with  $E_\beta > 10 \cdot 10^4$  erg/s cm<sup>2</sup> ster, where the  $H\beta$  profiles are saturated or even centrally reversed.

The mean Doppler widths of the observed metal lines amount to  $\Delta\lambda_D^{NaD_2} \approx 95$  and  $\Delta\lambda_D^{Mgb_2} \approx 82\text{ m\AA}$ , corresponding to  $\Delta\lambda_D/\lambda \approx 1.6 \cdot 10^{-5}$ . The narrow widths from this almost entirely non-thermal broadening yield  $v_{nth} \approx 5\text{ km/s}$ . Similarly narrow profiles of  $Mgb_2$  were reported by Landman (1985). Comparison with model calculations by Kim (1987; Fig. 7) indicates that these observations can only be reproduced with high total number densities up to  $N \leq 10^{12}\text{ cm}^{-3}$ .

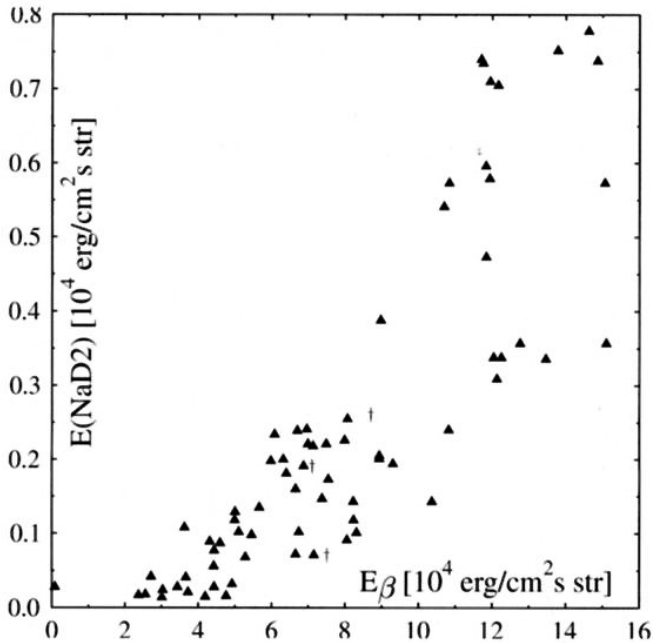


Fig. 9. Integrated intensity of NaD<sub>2</sub> versus that of H $\beta$ ; daggs show the observations by Yakovkin & Zel'dina (1963).

## 6. Conclusions

The present spectro-photometry extends our former analyses (Stellmacher & Wiehr 1994b, 1995) to four times higher H $\beta$  emissions. The here observed bright prominences are low latitude objects at  $\vartheta < 32^\circ$ . We find prominent central reversions of H $\alpha$  and occasionally of H $\beta$  for line radiance  $E_\beta > 5 \cdot 10^4$  erg/(s cm<sup>2</sup> ster). These centrally reversed profiles can well be modeled assuming semi-infinite layers, as is seen from a comparison with model calculations by Gouttebroze et al. (1993). The emitting layers should then consist of 'densely wound fibers forming massive ropes or wicks' (cf., Engvold 1998).

THEMIS proved to be a powerful instrument for multi-line spectral photometry, also useful for solar prominences. Due to its low stray-light level (seen in the rather faint aureole spectra) and its low instrumental polarization, one may extend these observations to filtergram techniques (cf., Stellmacher & Wiehr 2000) for a study of the dynamics of small-scale prominence structures inclusive their magnetic field as, e.g., done by Wiehr & Bianda (2003).

*Acknowledgements.* We thank the THEMIS team, in particular C. Briand for kind support. We are indebted to ENO for the grant 'THEMIS project No. 42'. The THEMIS telescope on Tenerife is operated by the French 'Centre National de la Recherche Scientifique' and the Italian 'Consiglio Nazionale delle Ricerche' at the Spanish 'Observatorio del Teide' of the Instituto de Astrofísica de Canarias.

## References

- Engvold, O. 1998, in (D. F. Webb, B. Schmieder, D. M. Rust, eds.) Proc. 'New Perspectives on Solar Prominences', IAU-coll. 167, 23  
 Gouttebroze, P., Heinzel, P. & Vial, J. C. 1993, A&AS 99, 513  
 Gouttebroze, P., Heinzel, P. & Vial, J. C. 1994, A&A 292, 656  
 Kim, K. S. 1987, Solar Phys. 114, 47  
 Labs, D. & Neckel, H. 1970, Solar Phys. 15, 79  
 Landman, D. A. 1985, ApJ 295, 220  
 Magnan, C. 1976, J. Quant. Spectrosc. Radial. Transfer 16, 281  
 Stellmacher, G. & Wiehr, E. 1994a, A&A 286, 302  
 Stellmacher, G. & Wiehr, E. 1994b, A&A 290, 665  
 Stellmacher, G. & Wiehr, E. 1995, A&A 299, 921  
 Stellmacher, G. & Wiehr, E. 1997, A&A 319, 669  
 Stellmacher, G. & Wiehr, E. 2000, Solar Phys. 196, 357  
 Stellmacher, G., Wiehr, E. & Dammasch, I. E. 2003, Solar Phys. 217, 133  
 Wiehr, E. & Bianda, M. 2003, A&A 404, L25  
 Yakovkin, N. A. & Zel'dina, M. Yu. 1963, Astron. Zh. 40, 847  
 Yakovkin, N. A. & Zel'dina, M. Yu. 1964, Astron. Zh. 41, 914